Dieses Dokument ist eine Zweitveröffentlichung (Postprint) /

This is a self-archiving document (accepted version):

Min Hyuk Park, Young Hwan Lee, Han Joon Kim, Yu Jin Kim, Taehwan Moon, Keum Do Kim, Seung Dam Hyun, Thomas Mikolajick, Uwe Schroeder, Cheol Seong Hwang

Understanding the formation of the metastable ferroelectric phase in hafnia–zirconia solid solution thin films

Erstveröffentlichung in / First published in:

Nanoscale. 2018, 10(2), S. 716-725 {Zugriff am: 11.10.2022}. RSC. ISSN 2040-3372.

DOI: https://doi.org/10.1039/C7NR06342C

Diese Version ist verfügbar / This version is available on:

https://nbn-resolving.org/urn:nbn:de:bsz:14-qucosa2-813361

SLUB Wir führen Wissen.

TECHNISCHE UNIVERSITÄT DRESDEN

QUCOSA Quality Content of Saxony

Final edited form was published in "Nanoscale. 2018, 10(2), S. 716-725. ISSN 2040-3372.
https://doi.org/10.1039/C7NR06342C

Understanding the formation of the metastable ferroelectric phase in hafnia–zirconia solid solution thin films†

Min Hyuk Park,[a,b] Young Hwan Lee,[a] Han Joon Kim,[a] Yu Jin Kim,[a] Taehwan Moon,[a] Keum Do Kim,[a] Seung Dam Hyun,[a] Thomas Mikolajick,[b,c] Uwe Schroeder,[b] Cheol Seong Hwang*[a]

$Hf_{1-x}Zr_xO_2$ ($x \sim 0.5$–0.7) has been the leading candidate of ferroelectric materials with a fluorite crystal structure showing highly promising compatibility with complementary metal oxide semiconductor devices. Despite the notable improvement in device performance and processing techniques, the origin of its ferroelectric crystalline phase (space group: $Pca2_1$) formation has not been clearly elucidated. Several recent experimental and theoretical studies evidently showed that the interface and grain bound-ary energies of the higher symmetry phases (orthorhombic and tetragonal) contribute to the stabilization of the metastable non-centrosymmetric orthorhombic phase or tetragonal phase. However, there was a clear quantitative discrepancy between the theoretical expectation and experiment results, suggesting that the thermodynamic model may not provide the full explanation. This work, therefore, focuses on the phase transition kinetics during the cooling step after the crystallization annealing. It was found that the large activation barrier for the transition from the tetragonal/orthorhombic to the monoclinic phase, which is the stable phase at room temperature, suppresses the phase transition, and thus, plays a critical role in the emergence of ferroelectricity.

Introduction

Since unexpected ferroelectricity in the doped-HfO_2 thin film was first reported in 2011,[1] research on the application of these complementary metal oxide semiconductor (CMOS) compatible materials in semiconductor memory devices has been actively reviving.[2–15] Among numerous doped fluorite structured materials that are shown to have ferroelectric (FE) properties, the HfO_2–ZrO_2 solid-solution ($Hf_{1-x}Zr_xO_2$) system is especially eye-catching.[7,9,11,14,16–18] This is because of the wide tunability of the material property from mostly dielectric ($x \sim 0$, pure HfO_2) to feasible ferroelectric ($x \sim 0.5$) to anti-ferroelectric-like (AFE, $x \sim 0.8$) to again dielectric with higher dielectric constant ($x \sim 1$, pure ZrO_2), of which precise performances are also film thickness-dependent.[16–18] It is generally accepted that the origin of ferroelectricity is the formation of the non-centrosymmetric orthorhombic phase (o-phase, space group: $Pca2_1$).[1,15,19] Sang *et al.* experimentally proved the existence of the ferroelectric o-phase based on a transmission electron diffraction (TEM) study.[19] However, the origin of the o-phase formation is not yet clearly understood. The o-phase is not a thermodynamically stable (regarding bulk-free energy) phase under typical processing conditions (room temperature–800 °C, several mbar–atmospheric pressure), whereas the monoclinic phase (m-phase, space group: $P2_1/c$) is always stable throughout all x-values.[20,21] Therefore, there must be other reasons for the emergence of the o-phase in thin films. An even more complicated finding is the dominant involvement of the tetragonal phase (t-phase, space group: $P4_2/nmc$) when the x-value is $\gtrsim 0.7$, which is not a stable phase either.[16,17] Materlik *et al.* suggested that the o-phase can be thermodynamically stabilized due to the surface energy effect.[22] They suggested that the bulk free energy and the surface energy of the o-phase are in between those of the m- and t-phases; so the o-phase can be stabilized in a particular thickness and grain size range for HfO_2 and $Hf_{0.5}Zr_{0.5}O_2$.[22] Nonetheless, more recent theoretical results by Batra *et al.* based on first principles calculation revealed that the expectation by Materlik *et al.* might not be correct.[23] Recently, some of the authors of this paper quantitatively compared the

[a]*Department of Materials Science & Engineering and Inter university Semiconductor Research Center, Seoul National University, Seoul 151 744, Korea.*
E mail: cheolsh@snu.ac.kr
[b]*NaMLab gGmbH, Noethnitzer Strasse 64, 01187 Dresden, Germany*
[c]*Chair of Nanoelectronic Materials, TU Dresden, 01062 Dresden, Germany*
†Electronic supplementary information (ESI) available. See DOI: 10.1039/c7nr06342c

Provided by Sächsische Landesbibliothek - Staats- und Universitätsbibliothek Dresden

Final edited form was published in "Nanoscale. 2018, 10(2), S. 716-725. ISSN 2040-3372.
https://doi.org/10.1039/C7NR06342C

experimental observations in their $Hf_{1-x}Zr_xO_2$ films with thicknesses ranging from 9.2 to 29.2 nm and x-values ranging from 0.0 to 1.0 with the modified surface energy model.[17] The essential contribution of this recent work is that the evolutions of the o-, t-, and m-phases as a function of composition and thickness, which determine the average grain size, could be expected from the available grain size data and suggested grain boundary energy values.[17] They also pointed out that the interface and grain boundary energy should be assumed to be ~1/3 of the surface energy.[17] In their results, the expected composition for the optimum FE performance from the interface and grain boundary energy was $x \sim 0.7$ for all tested thickness/grain size ranges, but experimental results showed that the best FE performance was always achieved for the films with $x \sim 0.5$.[17] The model based on the grain boundary energy effect indicated that the stable phase for the $x \sim 0.5$ films is the m-phase at room temperature (RT), at which the FE performances were observed.[17] Thus, they had to conclude that the o-phase crystalline nuclei, formed during the atomic layer deposition (ALD) of the $Hf_{1-x}Zr_xO_2$ film with a typical radius of ~2 nm, may retain their crystalline structure during post-metallization annealing (PMA) by rapid thermal annealing (RTA) at 500–650 °C, which then acted as the seed for full crystallization of the entire film.[17] However, how the phase transformation to the stable m-phase is suppressed during the crystallization annealing process was not elucidated. These results may suggest that the thermodynamic model itself may not be able to precisely explain the underlying mechanism of the FE phase evolution during the film deposition and RTA processes. The authors noted that the emergence of the stable phases could be highly dependent on the process temperature region, given the large contribution of the grain boundaries in such a nano-crystalline material system.

The estimation of the thermodynamically stable phase has been based on the grain size estimation and distribution of the films after crystallization by RTA. However, the films could have tiny sized, *in situ* crystallized nuclei (~2 nm radius) during the ALD step whose stable phase must be different from that of the finally crystallized grains (typical grain size $\gtrsim$5 nm radius) after the RTA step. Therefore, the presence of such initial nuclei at the as-deposited state and their influence on crystallization must be taken into account. Another critical ingredient for the phase evolution is the kinetic energy barrier for the phase transition. As will be discussed in detail in this work, the most probable initially crystallized phase during RTA at high temperature is the t-phase, whereas the thermodynamically stable phase at such high temperature is still the m-phase. Therefore, there is a driving force for the phase transition from the t- to the m-phase, but high kinetic barrier for such a transition may not allow it. The phase transition during the cooling step must also be considered because the phase stability of such nano-crystalline materials is far more sensitive to the temperature compared with the bulk materials, of which the stable phase is always the m-phase across the entire temperature range involved. In this study, therefore, the kinetic mechanism of how the crystalline phase is evolving during RTA and its transition to another phase during cooling in $Hf_{1-x}Zr_xO_2$ thin films is systematically examined. It could be concluded that the high kinetic barrier for the transition from the t-phase to the stable m-phase prohibits the undesirable phase transition. On the other hand, the transition from the t- to the o-phase could readily occur during cooling to RT due to the negligible energy barrier for that transition and stability of the o-phase at RT. In this work, based on these new insights, the phase evolution of the 9.2 nm thick $Hf_{1-x}Zr_xO_2$ films with x values of 0.5, 0.7 and 1.0 with the varying RTA temperature (400–800 °C) was examined. These new insights also provide the clue to solving the puzzle in the previous work of why the best FE performance was achieved in the composition of $x \sim 0.5$ and not from ~0.7.[17]

Experimental

The 9.2 ± 0.4 nm thick $Hf_{1-x}Zr_xO_2$ films were deposited on an SiO_2/Si substrate coated with a 50 nm thick TiN bottom electrode using thermal ALD at a substrate temperature of 280 °C. $Hf[N(C_2H_5)CH_3]_4$, $Zr[N(C_2H_5)CH_3]_4$, and ozone were used as a Hf-precursor, a Zr-precursor, and an oxygen source, respectively. The Zr/(Hf + Zr) ratios (x-values) were controlled by changing the ALD cycle ratio between the ALD processes for HfO_2 and ZrO_2. The growth rates of HfO_2 and ZrO_2 were both ~0.12 nm per cycle on a TiN electrode. Pt (60 nm)/TiN (20 nm) top electrodes were deposited using a shadow mask and magnetron sputtering for fabricating the capacitor samples (TiN contacts the $Hf_{1-x}Zr_xO_2$ film). After top electrode deposition, PMA was performed at 400–800 °C under a N_2 atmosphere by RTA for 30 s. The composition and the thickness of the $Hf_{1-x}Zr_xO_2$ films were examined using X-ray fluorescence (Quant'X, Thermo Scientific) and ellipsometry (L-116d, Gaertner), respectively. The grain size analysis was conducted using a watershed method implemented by Gwyddion software.[24] Polarization–electric field (P–E) characteristics were measured using a ferroelectric tester (TF analyzer 2000, Aixacct Systems) at a frequency of 1 kHz. The P–E curves were achieved from the non-woken up state to examine the pristine state. To analyze the crystalline structures, the grazing incidence X-ray diffraction (GIXRD) was conducted using an X-ray diffractometer (X'pert pro, Panalytical) equipped with a Cu Kα X-ray source. For the GIXRD measurement, the incidence angle was fixed at 0.5°, and the 2θ scan was conducted.

Results and discussion

First, the phase evolution with increasing RTA temperature for the $Hf_{1-x}Zr_xO_2$ films with x values of 0.5, 0.7 and 1.0 was examined using GIXRD. Fig. 1(a) shows the GIXRD patterns of 9.2 nm thick $Hf_{0.5}Zr_{0.5}O_2$ thin films annealed at various annealing temperatures from 400 to 800 °C, which were reproduced from the authors' previous study.[18] It showed that the intensity of the monoclinic-111 (m-111) diffraction peak ($2\theta \sim$

Provided by Sächsische Landesbibliothek - Staats- und Universitätsbibliothek Dresden

Final edited form was published in "Nanoscale. 2018, 10(2), S. 716-725. ISSN 2040-3372.
https://doi.org/10.1039/C7NR06342C

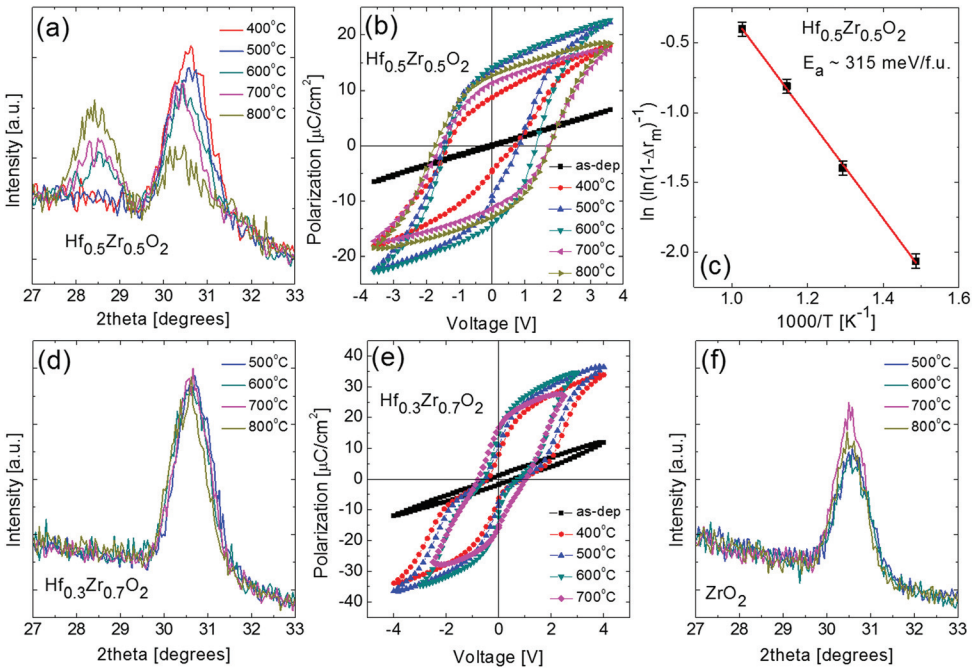

Fig. 1 (a) The grazing incidence X ray diffraction results (GIXRD) and (b) polarization electric field (*P E*) curves of 9.2 nm thick $Hf_{0.5}Zr_{0.5}O_2$ films. (c) An Arrhenius plot of the increase of the monoclinic phase fraction (Δr_m) *versus* 1000/*T* based on the Johnson Mehl Avrami model. The error bars show the areal errors from the Gaussian fittings. (d) The GIXRD results and (e) *P E* curves of 9.2 nm thick $Hf_{0.5}Zr_{0.5}O_2$ films. (f) The GIXRD results of the 9.2 nm thick ZrO_2 film.

28.5°) significantly increases while that of the orthorhombic 111/tetragonal 011 (o111/t011) peak ($2\theta \sim 30.5°$) decreases with increasing RTA temperature. The variations in the *P–E* curves shown in Fig. 1(b) are consistent with the GIXRD data. At the as-deposited state, the film was mostly amorphous containing tiny crystallites revealing almost linear dielectric properties with a dielectric constant of ~20.[18,25] With increasing RTA temperature from 400 to 600 °C, the film showed increased FE performance with a maximum $2P_r$ of ~30 μC cm^{-2} at 600 °C, although the GIXRD data in Fig. 1(a) showed a significant inclusion of the m-phase material. This seemingly contradictory result may be understood from the simultaneous crystallization of the amorphous material into the t-phase (which will then be transformed to the desired o-phase during cooling, as discussed later) and partial transformation of the t-phase to the m-phase during RTA for 30 s. With increasing RTA temperature up to 800 °C, the $2P_r$ value slightly decreased corroborating the increasing m-phase peak in GIXRD. Fig. 1(c) shows the result for the activation energy estimation according to the Johnson–Mehl–Avrami model. The m-phase fraction was calculated from the relative area intensity ratio of the m-phase diffraction peaks to the total summation of areal intensities of all the diffraction peaks in the 2θ range of 27–33°. It should be noted that this ratio does not necessarily reflect the actual m-phase portion in the film, but just the relative variation. The calculated activation energy from the least-square-linear-fitting of the data (red line) was 315 meV $f.u.^{-1}$, where f.u. stands for the formula unit, which may correspond to the activation energy of the phase transition from the t/o-phase to m-phase. The activation energy was calculated based on the assumptions that the phase transition from the t-phase or o-phase to the m-phase is a thermally activated process and that the transition process is dominated by a nucleation process rather than by grain growth. The details of the activation energy estimation are discussed in the ESI.†

The evolution of the phase and *P–E* curves in $Hf_{0.3}Zr_{0.7}O_2$ thin films according to different RTA temperatures, shown in Fig. 1(d) and (e), respectively, are quite different from the previous case. The film showed almost no involvement of the m-phase with increasing RTA temperature up to 800 °C but showed a slight shift of the o111/t011 peak position to the lower 2θ value with no intensity variation. This peak shift might be understood as reflecting the increased portion of the o-phase compared with that of the t-phase or the increased lattice parameter of the o/t-phases. The emergence of the distorted *P–E* curve in Fig. 1(e) indicates that the phase is mostly the t-phase at lower RTA temperature, but the increasing P_r value at higher RTA temperature suggests that a higher portion of the o-phase is present within the film. For the pure ZrO_2 case, shown in Fig. 1(f), there was no notable change in the GIXRD pattern, and its corresponding *P–E* curves (not shown) showed only a linear dielectric like behavior for all RTA temperatures with a typical dielectric constant of ~35. These results suggest that the ZrO_2 films retain almost a pure t-phase structure throughout the entire process conditions (ALD, RTA, and cooling).

Next, the thermodynamic model was invoked to explain these results. Here, the thermodynamic model refers to the stable

Provided by Sächsische Landesbibliothek - Staats- und Universitätsbibliothek Dresden

Final edited form was published in "Nanoscale. 2018, 10(2), S. 716-725. ISSN 2040-3372.
https://doi.org/10.1039/C7NR06342C

phase calculation based on the bulk and grain boundary/interface energies of each phase and the estimated grain size/distribution of the crystallized film. The grain boundary/interface energy was assumed to be 1/3 of the free surface energy. Details for such a calculation can be found elsewhere.[17]

Fig. 2(a)–(c) show the expected phase distribution from the thermodynamic model for the films with *x*-values of 0.5, 0.7, and 1.0, respectively, as a function of temperature and grain radius. The grain size distribution data were necessary upon drawing this diagram and were separately plotted in Fig. 3. Lightly shaded red, blue, and green regions indicate the range in which the most stable phases reside and were assigned to the o-, t-, and m-phases, respectively. It can be immediately noted that the m-phase has stability over the large grain size region. This must be a reasonable conclusion because higher symmetry phases (the t- and o-phases) with lower surface energy contribute less to the surface energy when the grain size is large. However, as the temperature increases, t-phase stability also increases, which can be understood from the higher entropy of this phase over that of the m- and o-phases by 210 (186) and 170 (162) kJ m^{-3} K^{-1} for HfO_2 (ZrO_2), respectively,[22] *i.e.*, the total free energy of the t-phase decreases rapidly with increasing temperature, whereas the enthalpy change was not very obvious. This is actually the reason why the bulk phase diagram also shows the transition from the m- to the t-phase at 1720 and 1170 °C for HfO_2 and ZrO_2, respectively.[26] There is a small region where the o-phase is stable in Fig. 2(a) and (b), which is not present in Fig. 2(c). Pure ZrO_2 has no driving force for the o-phase formation, which is consistent with the experimental results. This means that the phase and property evolution in ZrO_2 can be successfully explained solely by the thermodynamic model; so it will not be discussed anymore in this work.

However, the calculated grain size region where the o-phase is stable, indicated in Fig. 2(a) and (b), shows a significant inconsistency with the grain size region obtained from the actual experiment. The lateral red, green, and blue dotted lines in the figures indicate the boundary line of the grain radius above which 25, 50, and 75% of the grain size distribution within a sample were experimentally obtained. The arrows indicate the cooling process, and the obtained boundary region will be further discussed in Fig. 3. It can be immediately understood that the grain size range in the red shaded region, theoretically corresponding to the o-phase, is much below the experimentally achieved grain size range after RTA. Also, the experimentally achieved grain sizes reside mostly within the green shaded region, indicating that the dominant phase should be the m-phase at RT. Another problem is that the expected phase stability at higher temperatures is not consistent with the experimentally obtained stable phase, which can be more evidently seen in Fig. 3.

Fig. 3(a)–(c) and (d)–(f) show the stable phase estimation from the thermodynamic model for the given grain size distribution at three different temperatures for the $Hf_{0.5}Zr_{0.5}O_2$ and $Hf_{0.3}Zr_{0.7}O_2$ thin films, respectively. Here, the grain size distribution has been estimated from the scanning electron microscopy images of the differently annealed films, of which details can be found elsewhere.[17] The differently annealed films at different RTA temperatures with different compositions did not show any notable change in the average grain size distribution and the differences among each condition fell within the experimental errors. Therefore, the grain size distribution data from three different samples annealed at 500–700 °C were averaged and one representative distribution was used in Fig. 3 (see the ESI† for raw data). The grain size estimated from SEM does not necessarily coincide with the

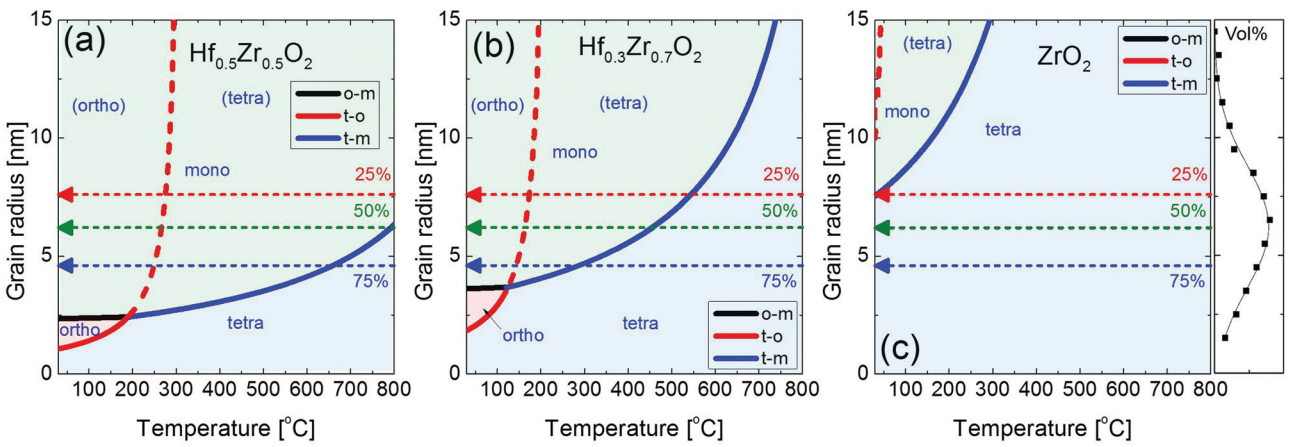

Fig. 2 The phase diagram of 9.2 nm thick (a) $Hf_{0.5}Zr_{0.5}O_2$, (b) $Hf_{0.3}Zr_{0.7}O_2$, and (c) ZrO_2 thin films with various grain size and temperatures. The light green, light blue, and light red regions refer to the regions where monoclinic, tetragonal, and orthorhombic phases are thermodynamically stable, respectively, with the interface/grain boundary energy effect. The phases in the parentheses refer to the second stable phase in the monoclinic phase region. The dashed red boundary shows the boundary at which the second stable phase changes. The red, green, and blue dashed arrows show the cooling down process during rapid thermal annealing (RTA) for grains with a radius smaller than 25, 50, and 75% of the grains. The panel on the right side of (c) shows the grain size distribution from SEM images for better understanding the meaning of the dashed arrows (mono: monoclinic; tetra: tetragonal; ortho: orthorhombic; vol%: volumetric fraction in %).

Provided by Sächsische Landesbibliothek - Staats- und Universitätsbibliothek Dresden

Final edited form was published in "Nanoscale. 2018, 10(2), S. 716-725. ISSN 2040-3372.
https://doi.org/10.1039/C7NR06342C

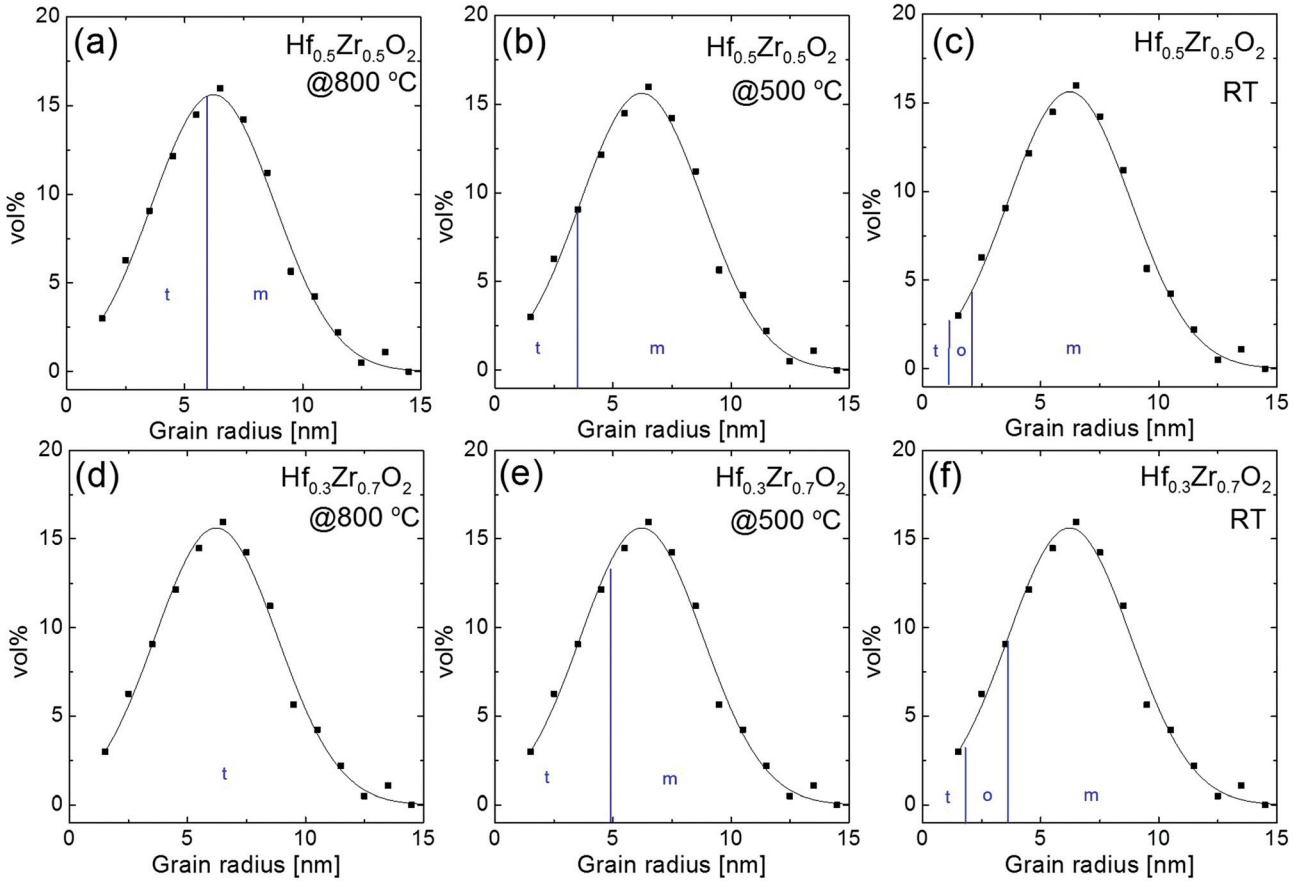

Fig. 3 The grain size distribution with the critical grain size (blue vertical lines) for the phase change of the 9.2 nm thick $Hf_{0.5}Zr_{0.5}O_2$ film at (a) 800 °C, (b) 500 °C, and (c) room temperature, respectively. The grain size distribution with the critical grain size (blue vertical lines) for the phase change of the 9.2 nm thick $Hf_{0.3}Zr_{0.7}O_2$ film at (a) 800 °C, (b) 500 °C, and (c) room temperature, respectively.

crystallographic grain size which can be analyzed using transmission electron microscopy (TEM). However, it was confirmed previously that the grain size from SEM and TEM was fairly consistent for the atomic layer deposited $Hf_{1-x}Zr_xO_2$ thin films, and columnar grains could be confirmed.[27] The m-phase should be stabilized as the grain radius becomes larger at a given temperature, which was coincident with the experimental data, shown in Fig. 3(a)–(f). With increasing temperature or *x*-value, the area of the stable t-phase region increases, due to the entropy and interface/grain boundary energy effect, respectively, which is also visible in the same figure. For the $Hf_{0.3}Zr_{0.7}O_2$ film at 800 °C, the entire film is stabilized in the t-phase.

Although the phase evolution trend from the grain size difference with respect to the temperature and the Zr composition is logically coherent, some discrepancies between the theoretical and experimental phases are evident. When the theoretical expectation on the stabilized phase and the experimentally obtained results were compared for the $Hf_{0.5}Zr_{0.5}O_2$ film, the film should theoretically be composed almost entirely of the m-phase at RT, and on increasing the temperature, the m-phase portion should decrease. This is in a stark contrast to the experimental results shown in Fig. 1. In the experiment, the m-phase formation was actually suppressed and the o-phase became dominant at lower RTA temperature, whereas the m-phase dominance at higher RTA temperature was qualitatively consistent. Even though the o-phase cannot be distinguished from the t-phase solely based on GIXRD, the dominant crystalline phase at lower RTA temperatures could be identified as the o-phase from the *P*–*E* characteristics in Fig. 2b.

Various factors other than interface/grain boundary energy which can potentially affect the free energy of each phase were also carefully considered. According to previous work by Hoffmann *et al.*,[28] oxygen vacancies decrease the free energy of the orthorhombic and tetragonal phase further by −15 and −24 meV f.u.$^{-1}$, when 6.25% of oxygen vacancies are present in Gd-doped HfO_2 thin films. With the assumption that the effect of oxygen vacancies is the same in the $Hf_{1-x}Zr_xO_2$ thin films, the free energy of the t-phase further decreases compared to the o-phase and m-phase by 9 and 24 meV f.u.$^{-1}$, respectively. This means that the t-phase to o-phase and the t-phase to m-phase transitions are expected to occur at temperatures even lower than the result presented in Fig. 2. It was suggested that the oxygen vacancy concentration is higher at the interfacial region between the ferroelectric doped HfO_2 film and the TiN

Provided by Sächsische Landesbibliothek - Staats- und Universitätsbibliothek Dresden

Final edited form was published in "Nanoscale. 2018, 10(2), S. 716-725. ISSN 2040-3372.
https://doi.org/10.1039/C7NR06342C

electrode because TiN partly reduces the HfO_2 film at the interface.[28,29] A similar effect is expected in the HZO film considering the comparable chemical natures of HfO_2 and ZrO_2. Thus, the oxygen vacancy concentration in $Hf_{1-x}Zr_xO_2$ thin films should be higher when the film is annealed at higher temperature, and a higher t-phase fraction is expected, which is inconsistent with the experiment. Thus, the changes in the relative fractions of each phase cannot be explained based on the effect of oxygen vacancies.

Film stress is also suggested to potentially affect the free energy of each crystalline phase in $Hf_{1-x}Zr_xO_2$ thin films. Shiraishi *et al.*[30] examined the in-plane stress in $Hf_{0.5}Zr_{0.5}O_2$ thin films deposited on various substrates with different coefficients of thermal expansion (CTE) and suggested that a lower m-phase portion is formed when a higher in-plane tensile stress is present in $Hf_{0.5}Zr_{0.5}O_2$ thin films. The thermal stress in thin films can be estimated by multiplying the CTE difference between the $Hf_{1-x}Zr_xO_2$ film and the substrate by the difference between the annealing temperature and RT. The CTE of $Hf_{1-x}Zr_xO_2$ (10.0×10^{-6} per °C) is higher than that of Si (4.5×10^{-6} per °C);[30] so a higher tensile stress is expected when the $Hf_{1-x}Zr_xO_2$ film is annealed at higher temperature. Thus, a lower m-phase fraction is expected for the $Hf_{1-x}Zr_xO_2$ thin film annealed at higher temperature, which is inconsistent with the experimental observations. Therefore, the stress effect cannot explain the experimental results.

The effect of diffusion of Ti and N was also considered as a potential cause for m-phase formation. However, both Ti and N were reported to stabilize meta-stable phases.[31–33] Xu *et al.* showed that N can stabilize the o- and t-phases.[33] Ti is known to be not an effective t-phase stabilizer, but disclosed to decrease the t-phase energy compared to that of the m-phase.[32,33] Thus, the increased fraction of the m-phase cannot be understood based on the diffusion of Ti and N. In order to understand the aforementioned discrepancy, the probable crystallization steps in the experimental processes (ALD, RTA, and cooling) were modeled in Fig. 4. During ALD (Fig. 4(a)), there will be almost no kinetic barrier for the formation of crystalline nuclei because of the very high surface mobility of the adsorbed atoms on the surface meaning that the thermodynamic effect, *i.e.*, bulk and surface free energies, will dominantly determine the phase. However, the crystallite size will be limited to a very small value (~2 nm radius in this study) due to the low ALD temperature (280 °C). The interfaces with the electrode might provide the preferable sites for the crystalline nuclei, but for the sake of simplicity of the following estimation, the nuclei were assumed to be randomly distributed within the amorphous matrix in the as-deposited state in Fig. 2a. Even if heterogeneous nucleation were assumed, the conclusion would not critically be influenced. From Fig. 2(a), it can be noted that the stable phase of such tiny nuclei at 280 °C is the t-phase. They could be transformed into the o-phase when the sample is taken out from the ALD chamber to the atmosphere before loading it into the RTA chamber. However, as can be expected from the same figure, it will transform to the t-phase again at the RTA temperature. During RTA at temperatures up to 800 °C, these t-phase nuclei would work as the seed for the heterogeneous nucleation of the amorphous matrix phase, as depicted in Fig. 4(b) and (c). According to the thermodynamic expectation shown in Fig. 3(b) and (c), most of the crystallized grains should possess the m-phase with a marginal amount of the t-phase at 500 °C. At 800 °C, there should be approximately equal portions of the m- and t-phases. In any case, there is no room for the stabilized o-phase. These findings are inconsistent with the experimental results where the o-phase and the m-phase were dominant, and their portion actually increased with increasing temperature. The probable answer to this problem can be found from the kinetic point of view, where the transition from the supposedly t- to m-phase is kinetically hindered by a high activation barrier of such a transition. In fact, the high activation energy estimated in Fig. 1(c) already indicates that such a phase transition from the t- to the m-phase must be quite sluggish.

The kinetic energy barrier can be calculated from the general phase transition theory at the critical nucleus size, of which details are included in the ESI† where the bulk free energy, interface/grain boundary energy, and mechanical energy related with the strain are taken into consideration. The estimated activation barrier for the t- to m-phase transition was 223–262 meV f.u.$^{-1}$, which is quite comparable to the activation energy of 315 meV f.u.$^{-1}$ in Fig. 1(c). The experimentally estimated activation energy was higher than the theoretically calculated values, but it should be noted that the theoretical values were calculated based on only elastic and interfacial energies. Meanwhile, the activation energy for the t- to o-phase can be similarly calculated, which was only 22–31 meV f.u.$^{-1}$ These values are close to the reported values from other studies (~208 meV f.u.$^{-1}$[34] for t → m; and ~30 meV f.u.$^{-1}$ for t → o).[22,35–37] From these considerations, it can be assumed that the phase transition from the t- to m-phase during RTA can be kinetically suppressed while its driving force keeps increasing with decreasing temperature. The relative phase transition rate (R^*) can be estimated from its exponential dependency on the critical nucleation barrier (ΔG^*) and temperature (T) as $R^* \sim \exp(-\Delta G^*/kT)$, where k is the Boltzmann constant. Fig. 5(a) and (b) show the variation in the relative stability portion of the m-phase (black line; this can be calculated by integrating the area under the grain size distribution curves as plotted as the m-phase in Fig. 3) and exp ($-\Delta G^*/kT$) (red line), and their product, respectively, as a function of T. This variation qualitatively explains the phase evolution of the m-phase as a function of RTA temperature shown in Fig. 1(a). The increase in the m-phase portion with increasing temperature is due to the increased transformation rate from the t- to the m-phase which is large enough to over-compensate the driving force for the m- to t-phase transition as temperature rises.

However, this still does not explain the evolution of the o-phase and FE performance at RT. It must be reminded that there could be a significant portion of the t-phase still remaining during the RTA processes, even after allowing the kinetically limited m-phase formation in Fig. 5. Therefore, the

Provided by Sächsische Landesbibliothek - Staats- und Universitätsbibliothek Dresden

Final edited form was published in "Nanoscale. 2018, 10(2), S. 716-725. ISSN 2040-3372.
https://doi.org/10.1039/C7NR06342C

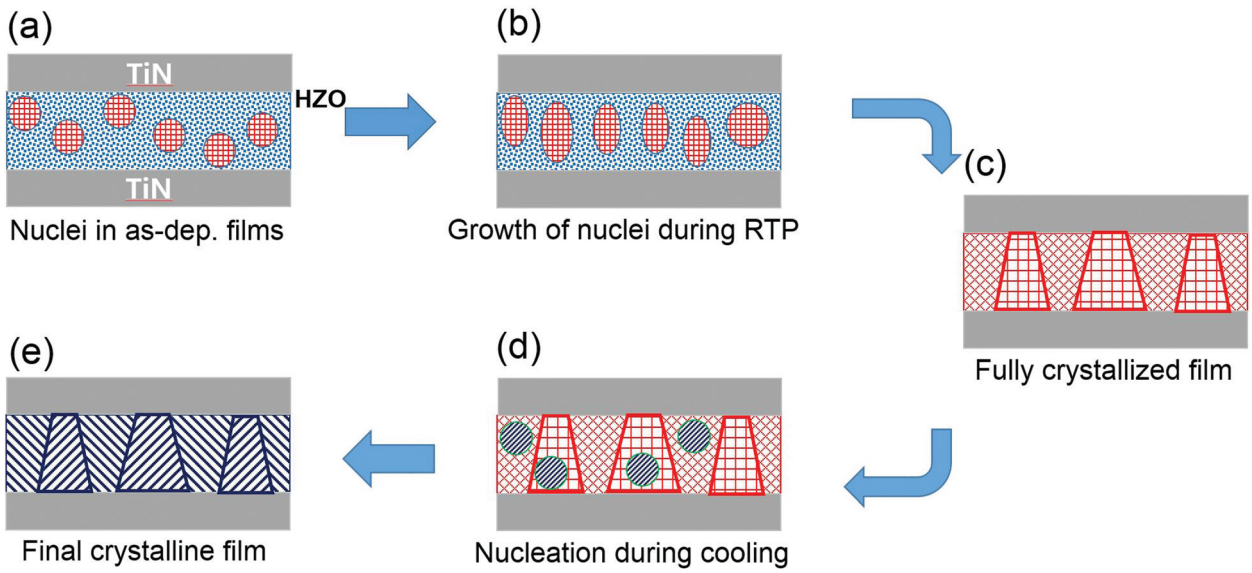

Fig. 4 The schematic diagram of the crystallization and phase transition considered in this paper. (a) The as deposited films with nanocrystallites. (b) The growth process of nuclei at high temperature during rapid thermal annealing (RTA). (c) The fully crystalline film during RT. (d) The nucleation of the low temperature stable phase during cooling down. (e) The final crystalline phase after RTA.

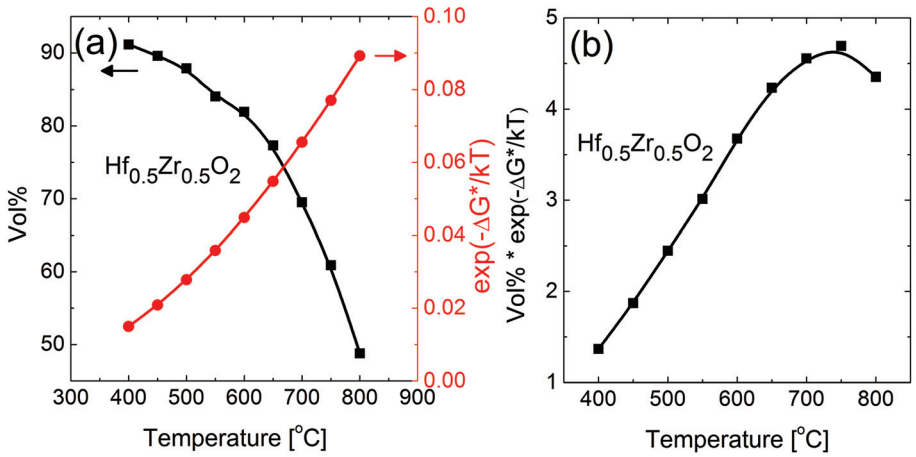

Fig. 5 The change of volumetric % for monoclinic phase stabilization (left black *y* axis) and exp($\Delta G^*/kT$) (right red *y* axis) as functions of tempera ture for the $Hf_{0.5}Zr_{0.5}O_2$ thin film. (b) The change of volumetric % for monoclinic phase stabilization multiplied by exp($\Delta G^*/kT$) for the $Hf_{0.5}Zr_{0.5}O_2$ thin film (ΔG^*: activation energy for the tetragonal to monoclinic phase transition).

remaining t-phase can be transformed to the o-phase during cooling. Because the entropy of the t-phase is slightly higher than that of the o-phase, the t-phase is still the high-temperature phase for the given grain size. What the dashed curve in Fig. 2(a) in the (supposedly) m-phase region indicates is the boundary between the t- and o-phases once the m-phase formation is kinetically suppressed. Hence, all of the remaining t-phases after RTA can be transformed to the o-phase at a temperature around 250–300 °C during cooling since the low kinetic barrier allows it. As discussed above, the kinetic barrier for such a transition is only ~1/9–1/7 of that for the t- to m-phase transition, which can be readily overcome by the thermal energy in this temperature region. Fig. 4(d) and (e) show such a transition during cooling. The large and small activation energies for the t- to m-phase and the t- to o-phase can be understood from the large and small differences in involved lattice structures. Therefore, the evolution of the crystalline phase and *P–E* curves with increasing RTA temperature shown in Fig. 1(a) and (b), and the emergence of the FE phase despite the thermodynamic stability of the m-phase at RT for the case of $Hf_{0.5}Zr_{0.5}O_2$ [ref. 17] can be understood in this way. It should be noted that the m-phase once transformed at high temperatures cannot be transformed to the o-phase during cooling because the m-phase has become the stable phase, which is the reason why the significant m-phase portion can be detected at RT in Fig. 1(a).

Provided by Sächsische Landesbibliothek - Staats- und Universitätsbibliothek Dresden

Final edited form was published in "Nanoscale. 2018, 10(2), S. 716-725. ISSN 2040-3372.
https://doi.org/10.1039/C7NR06342C

Next, the phase evolution and the *P–E* curves for the $Hf_{0.3}Zr_{0.7}O_2$ films are discussed. First, the non-emergence of the m-phase across the entire RTA temperature region can be similarly understood from the aforementioned kinetic barrier for the t- to m-phase transition, combined with even higher stability of the t-phase in this composition (Fig. 2(b) and 3(d)–(f)). It seems that the probability of the m-phase formation, in this case, is minimal. Nonetheless, the second stable phase for all grain sizes at RT even in this composition (stable m-phase formation is kinetically prohibited) is the o-phase as can be understood from Fig. 2(b), whereas the experiment indicated that the actual film at RT consists mostly of the t-phase. Therefore, the involvement of the retaining t-phase might be understood from the limited transition from the t- to the o-phase by a kinetic barrier at an even lower temperature of ~150–200 °C in this case. When a similar activation barrier was assumed (25 meV f.u.$^{-1}$), however, a temperature difference of ~100 °C (compared with the case of the $Hf_{0.5}Zr_{0.5}O_2$ film of which the t- to o-phase transition may occur at 250–300 °C) results in the transition rate difference of only 10–20%. Therefore, it seems that this difference is insufficient to explain the suppression of the o-phase formation kinetically. Thus, there might be some other mechanism that can lower the free energy of the t-phase compared to the o-phase. One possible explanation might be the stress state in thin films. The unit cell volume of the t-phase is smaller than that of the o-phase by about 2%. Therefore, if the unit cell volume of the t-phase film is lowered by the stress effect, the t-phase stability might be enhanced. In the GIXRD patterns in Fig. 1(d), the t-011 peak location is 30.6°. From the bulk lattice parameters at 1250 °C (a = 0.364 nm, c = 0.527 nm)[38] and thermal expansion coefficient (TEC, a-TEC: 10×10^{-6} per °C, c-TEC: 15×10^{-6} per °C) the t-011 peak location is expected to be 30.3°.[39] The volume difference of 0.5% between tetragonal HfO_2 and ZrO_2 suggests that the unit cell volume of $Hf_{0.3}Zr_{0.7}O_2$ might be about 0.15% smaller than that of ZrO_2.[22] This simple calculation indicates that the unit cell volume of the thin $Hf_{0.3}Zr_{0.7}O_2$ film in this work is ~2.7% smaller compared to that of the bulk counterpart. This decreased unit cell volume in the thin film might decrease the overall free energy of the t-phase compared to the o-phase, and suppress the phase transition to the o-phase.

Now, the remaining question is why the o-phase portion increases with increasing RTA temperature. It should be noted that the o-phase cannot be distinguished from the t-phase solely by GIXRD, but an increase in P_r with increasing annealing temperature strongly implies the increasing fraction of the o-phase. This might be understood from a similar argument based on the unit cell volume. As previously mentioned, the t-011 diffraction peak shifts to the low 2θ angle, implying a volume increase with increasing annealing temperature. It was already mentioned that the unit cell volume of the thin $Hf_{0.3}Zr_{0.7}O_2$ film is ~2.7% smaller compared to the bulk value. With increasing annealing temperature, this volume difference decreases, suggesting that the free energy lowering effect of the t-phase compared to the o-phase becomes lessened. As a result, the t- to o-phase transition might increase. While the o- to t-phase transition temperature has an increasing tendency with increasing grain size (see Fig. 3(b)), the increased lattice parameter of the film annealed at higher RTA temperature will shift the overall transition temperature to a higher value. Therefore, during cooling after RTA, the film with higher RTA temperature would experience the t- to o-phase transition at a higher temperature, which will kinetically increase the o-phase portion. This mechanism can solve the final puzzle of increasing o-phase portion with increasing RTA temperature in this composition film.

In conclusion, a plausible kinetic model for the emergence of the ferroelectric o-phase in $Hf_{0.5}Zr_{0.5}O_2$ films and the antiferroelectric like t-phase in $Hf_{0.3}Zr_{0.7}O_2$ films is suggested based on the high (~300 meV f.u.$^{-1}$) and low (~30 meV f.u.$^{-1}$) activation energy barrier for the t- to m-phase and the t- to o-phase transitions, respectively. The thermodynamic model considering the bulk and grain boundary/interface energy effects indicated that the m-phase is always the most stable phase at most RTA temperatures and the resulting grain sizes for the $Hf_{0.5}Zr_{0.5}O_2$ films. However, the tiny nuclei (~2 nm radius) formed *in situ* during ALD will most probably have the t-phase structure, which will serve as the crystallization seed of the entire film into the t-phase during RTA. The supposed transition to the m-phase at the achieved grain size would be suppressed by the high activation barrier, and the retained t-phase would be changed to the desired o-phase during cooling. At excessively high RTA temperature (>700 °C), the transition to the m-phase was kinetically enhanced, while the stability of the m-phase decreases thermodynamically at high temperature. The combined effect can explain the increasing portion of the m-phase with increasing RTA temperature.

For the case of the $Hf_{0.3}Zr_{0.7}O_2$ films, the thermodynamic stability of the m-phase decreases whereas the t-phase stability increases due to the composition effect. Nonetheless, the m-phase was still calculated to be the most stable phase over a large RTA temperature range; so the kinetic limitation to the m-phase must also be invoked. Another critical point of this composition is that the transition temperature for the t- to o-phase is lower than that for the $Hf_{0.5}Zr_{0.5}O_2$ film by ~100 °C. This also makes this transition kinetically limited, despite the fact that the second stable phase (given that the m-phase transition was completely suppressed) is also the o-phase. However, this effect is estimated to be only 10–20%, implying that it is not sufficient to explain the o-phase suppression. Compared to the bulk $Hf_{0.3}Zr_{0.7}O_2$, the unit cell volume of the thin $Hf_{0.3}Zr_{0.7}O_2$ film in this study is smaller by 2.7% compared with the bulk material. This volume decrease is expected to lower the free energy of the t-phase compared to that of the o-phase, and it would suppress the t- to o-phase transition. These combined thermodynamic–kinetic models can feasibly explain the experimental observations which could not be precisely explained by the previous thermodynamic model alone. This work also hints that the final phase after ALD–RTA–cooling could be critically dependent on the detailed process conditions, even including the cooling rate, which has not been appropriately addressed experimentally.

Provided by Sächsische Landesbibliothek - Staats- und Universitätsbibliothek Dresden

Final edited form was published in "Nanoscale. 2018, 10(2), S. 716-725. ISSN 2040-3372.
https://doi.org/10.1039/C7NR06342C

Conflicts of interest

There are no conflicts to declare.

Acknowledgements

C. S. H. acknowledges support from the Global Research Laboratory Program (2012 K1A1A2040157) of the Ministry of Science, ICT, and Future Planning and a grant from the National Research Foundation of Korea (NRF) (No. NRF-2014R1A2A1A10052979). M. H. P. is supported by a Humboldt postdoctoral fellowship from the Alexander von Humboldt Foundation.

References

1 T. S. Böscke, J. Müller, D. Bräuhaus, U. Schröder and U. Böttger, *Appl. Phys. Lett.*, 2011, **99**, 102903.
2 S. Mueller, S. R. Summerfelt, J. Müller, U. Schroeder and T. Mikolajick, *Electron Device Lett.*, 2012, **33**, 1300.
3 T. Mikolajick, S. Müller, T. Schenk, E. Yurchuk, S. Slesazeck, U. Schröder, S. Flachowsky, R. van Bentum, S. Kolodinski, P. Polakowski and J. Müller, *Adv. Sci. Technol.*, 2014, **95**, 136–145.
4 J. Müller, E. Yurchuk, J. Paul, R. Hoffmann, S. Müller, D. Martin, S. Slesazeck, P. Polakowski, J. Sundqvist, M. Czernohorsky, K. Seidel, P. Kücher, R. Boschke, M. Trentzsch, K. Gebauer, U. Schröder and T. Mikolajick, in Symp. on VLSI Technology Digest of Technical Papers, 2012, p. 25.
5 J. Müller, T. S. Böscke, Y. Yurchuk, P. Polakowski, J. Paul, D. Martin, T. Schenk, K. Khullar, A. Kersch, W. Weinreich, S. Riedel, K. Seidel, A. Kumar, T. M. Arruda, S. V. Kalinin, T. Schlosser, R. Boschke, R. van Bentum, U. Schröder and T. Mikolajick, in IEEE International Electron Devices Meeting, 2013, p. 10.8.1.
6 M. Hoffmann, M. Pešić, K. Chatterjee, A. I. Khan, S. Salahuddin, S. Slesazeck, U. Schroeder and T. Mikolajick, *Adv. Funct. Mater.*, 2016, **26**, 8643.
7 M. H. Park, H. J. Kim, Y. J. Kim, T. Moon, K. D. Kim and C. S. Hwang, *Nano Energy*, 2015, **12**, 131–140.
8 M. Hoffmann, U. Schroeder, C. Künneth, A. Kersch, S. Starschich, U. Böttger and T. Mikolajick, *Nano Energy*, 2015, **18**, 154.
9 M. H. Park, H. J. Kim, Y. J. Kim, T. Moon, K. D. Kim, Y. H. Lee, S. D. Hyun and C. S. Hwang, *Adv. Mater.*, 2016, **28**, 7956.
10 M. H. Park, T. Schenk, M. Hoffmann, S. Knebel, J. Gartner, T. Mikolajick and U. Schroeder, *Nano Energy*, 2017, **36**, 381.
11 M. H. Park, H. J. Kim, Y. J. Kim, T. Moon, K. D. Kim and C. S. Hwang, *Adv. Energy Mater.*, 2014, **4**, 201400610.
12 M. Pešić, M. Hoffmann, C. Richter, T. Mikolajick and U. Schroeder, *Adv. Funct. Mater.*, 2016, **26**, 7486.
13 P. D. Lomenzo, C.-C. Chung, C. Zhou, J. L. Jones and T. Nishida, *Appl. Phys. Lett.*, 2017, **110**, 232904.
14 K. D. Kim, Y. H. Lee, T. Gwon, Y. J. Kim, H. J. Kim, T. Moon, S. D. Hyun, H. W. Park, M. H. Park and C. S. Hwang, *Nano Energy*, 2017, **39**, 390.
15 M. H. Park, Y. H. Lee, H. J. Kim, Y. J. Kim, T. Moon, K. D. Kim, J. Müller, A. Kersch, U. Schroeder, T. Mikolajick and C. S. Hwang, *Adv. Mater.*, 2015, **27**, 1811.
16 J. Müller, T. S. Böscke, U. Schröder, S. Mueller, D. Bräuhaus, U. Böttger, L. Frey and T. Mikolajick, *Nano Lett.*, 2012, **12**, 4318.
17 M. H. Park, Y. H. Lee, H. J. Kim, T. Schenk, W. Lee, K. D. Kim, F. P. G. Fengler, T. Mikolajick, U. Schroeder and C. S. Hwang, *Nanoscale*, 2017, **9**, 9973.
18 M. H. Park, H. J. Kim, Y. J. Kim, W. Lee, T. Moon and C. S. Hwang, *Appl. Phys. Lett.*, 2013, **102**, 242905.
19 X. Sang, E. D. Grimley, T. Schenk, U. Schröder and J. M. LeBeau, *Appl. Phys. Lett.*, 2015, **106**, 162905.
20 O. Ohtaka, H. Fukui, T. Kunisada, T. Fujisawa, K. Funakoshi, W. Utsumi, T. Irifune, K. Kuroda and T. Kikegawa, *J. Am. Ceram. Soc.*, 2001, **84**, 1369–1373.
21 O. Ohtaka, H. Fukui, T. Kunisada, T. Fujisawa, K. Funakoshi, W. Utsumi, T. Irifune, K. Kuroda and T. Kikegawa, *Phys. Rev. B: Condens. Matter Mater. Phys.*, 2001, **63**, 174108.
22 R. Materlik, C. Künneth and A. Kersch, *J. Appl. Phys.*, 2015, **117**, 134109.
23 R. Batra, H. D. Tran and R. Ramprasad, *Appl. Phys. Lett.*, 2016, **108**, 172902.
24 D. Nečas and P. Klapetek, *Cent. Eur. J. Phys.*, 2012, **10**, 181–188.
25 M. H. Park, *Novel material and device for ferroelectric memory: thin $Hf_{1-x}Zr_xO_2$ film and tri-states memory*. Ph.D. thesis, Seoul National University, Republic of Korea, 2014.
26 F. Cardarelli, *Materials Handbook*, Springer, London, 2000.
27 K. D. Kim, M. H. Park, H. J. Kim, Y. J. Kim, T. Moon, Y. H. Lee, S. D. Hyun, T. Gwon and C. S. Hwang, *J. Mater. Chem. C*, 2016, **4**, 6864.
28 M. Hoffmann, U. Schroeder, T. Schenk, T. Shimizu, H. Funakubo, O. Sakata, D. Pohl, M. Drescher, C. Adelmann, R. Materlik, A. Kersch and T. Mikolajick, *J. Appl. Phys.*, 2015, **118**, 072006.
29 M. Pešić, F. P. G. Fengler, L. Larcher, A. Padovani, T. Schenk, E. D. Grimley, X. Sang, M. LeBeau, S. Slesazeck, U. Schroeder and T. Mikolajick, *Adv. Funct. Mater.*, 2016, **26**, 4601.
30 T. Shiraishi, K. Katayama, T. Yokouchi, T. Shimizu, T. Oikawa, O. Sakata, H. Uchida, T. Kiguchi and H. Funakubo, *Appl. Phys. Lett.*, 2016, **108**, 262904.
31 C.-K. Lee, E. Cho, H.-S. Lee, C. S. Hwang and S. Han, *Phys. Rev. B: Condens. Matter Mater. Phys.*, 2008, **78**, 012102.
32 D. Cunningham, A First-Principles Examination of Dopants in HfO_2, Honors Scholar Theses, 359, University of Connecticut, 2014, http://opencommons.uconn.edu/srhonors_theses/359.

Provided by Sächsische Landesbibliothek - Staats- und Universitätsbibliothek Dresden

Final edited form was published in "Nanoscale. 2018, 10(2), S. 716-725. ISSN 2040-3372.
https://doi.org/10.1039/C7NR06342C

33 L. Xu, T. Nishimura, S. Shibayama, T. Yajima, S. Migita and A. Toriumi, *Appl. Phys. Express*, 2016, **9**, 091501.
34 B. M. Hudak, S. W. Depner, G. R. Waetzig, A. Talapatra, R. Arroyave, S. Banerjee and B. S. Guiton, *Nat. Commun.*, 2017, **8**, 15316.
35 S. E. Reyes-Lillo, K. F. Garrity and K. M. Rabe, *Phys. Rev. B: Condens. Matter Mater. Phys.*, 2014, **90**, 140103.
36 T. D. Huan, V. Sharma, G. A. Rossetti and R. Ramprasad, *Phys. Rev. B: Condens. Matter Mater. Phys.*, 2014, **90**, 064111.
37 M. H. Park, H. J. Kim, Y. J. Kim, Y. H. Lee, T. Moon, K. D. Kim, S. D. Hyun and C. S. Hwang, *Appl. Phys. Lett.*, 2015, **107**, 192907.
38 G. Teufer, *Acta Crystallogr.*, 1962, **15**, 1187.
39 R. P. Haggerty, P. Sarin, Z. D. Apostolov, P. E. Driemeyer and W. M. Kriven, *J. Am. Ceram. Soc.*, 2014, **97**, 2213–2222.

Provided by Sächsische Landesbibliothek - Staats- und Universitätsbibliothek Dresden